ADVANCED FUNCTIONAL MATERIALS
www.afm-journal.de

Methods and Applications of Multilayer Silk Fibroin Laminates Based on Spatially Controlled Welding in Protein Films

*Mark A. Brenckle, Benjamin Partlow, Hu Tao, Matthew B. Applegate, Andrew Reeves, Mark Paquette, Benedetto Marelli, David L. Kaplan, and Fiorenzo G. Omenetto**

Recent use of biopolymers as interface materials between planar, inorganic electronics and biological tissues has required the adaptation of micro- and nanofabrication techniques for use with these nontraditional materials. In this work, a method which builds on this principle for spatial control of adhesion in multilayer silk fibroin laminates is investigated. This is accomplished through the addition of a spatially patterned amorphous silk adhesive layer in between the films to be adhered, before thermally processing them with heat (120 °C) and pressure (80 Psi) according to established procedures. A one-step method for rapid, high-throughput fabrication is demonstrated, which establishes a strong (1100 kPa) bond between the layers independent of the initial processing conditions of the films. The adhesive layers can be patterned using existing silk fabrication techniques, allowing for the assembly of complex geometries including bilayers and microbubbles. Additionally, the utility of this method is demonstrated for potential applications in drug delivery and transient electronics. This approach provides a versatile method for construction of complex multilayer structures in silk, which with future work may ultimately improve the utility of this material as a bridge between high technology and the biomedical sciences.

1. Introduction

The increasingly prevalent application of high technology to medical devices has led to a number of new materials challenges, in seeking to interface the soft, wet, curvilinear surfaces of biological tissues with the hard, dry, planar ones of conventional electronics and optics. Approaches to this interface problem have ranged from geometry and fabrication-driven strategies using conventional materials to the adaptation of polymers to electronic ends.[1–6] As a hybrid between these two approaches, silk fibroin protein from the *Bombyx mori* silkworm has recently found use as a bridge between electronic and biological fields.[7] The biocompatibility, resorbability, and mechanical properties of this material have made it effective in use as a bioelectronic substrate, optical sensor, and drug delivery vehicle.[8–14] Adaptation for use with common micro- and nanofabrication techniques has further enhanced the utility of silk in these areas, including recent work leveraging the variable glass transition temperature (T_g) in amorphous (i.e., noncrystalline) fibroin films for thermal fabrication methods.[15–19]

The variable T_g in silk is due to the plasticizing effect of water within the matrix of an amorphous silk film, and scales inversely with the water content in the film.[20] It varies over a wide range, from 178 °C for pure silk protein to approximately room temperature for films cast at ambient conditions, which are above 20% water by mass. Previous work has shown that rapid application of heat (above T_g) and pressure causes a film to crystallize into a high beta-sheet secondary structure.[17,19,21]

During this process, silk films pass through an intermediate viscoelastic liquid state in what has been termed the silk fibroin "reflow mechanism," which can lead to either imprinting or adhesion. Adhesion occurs due to the formation of a weld from interdiffusion of the two silk layers.[19,21] The amount of layer interdiffusion in the welded laminates is dependent on the crystalline state and water content of the individual films. Wet, amorphous silk films have a high viscoelastic reflow potential and an ability to form strong bonds, in contrast to dry, precrystallized films, which have previously shown little silk/silk adhesion.[19]

In this work, we investigate a method that builds on this mechanism to spatially control adhesion in multilayer silk laminates, independent of the initial processing conditions of the films. This is accomplished through the addition of a spatially patterned silk adhesive layer between the films to be bonded (**Figure 1**). The silk adhesive layer is amorphous in all cases, which should allow it to reflow into both films and initiate a bond. Alternately referred to as "lamination," this improved welding method should enable fabrication of devices in more than two layers, and increase the achievable device geometries

M. A. Brenckle, B. Partlow, Prof. H. Tao,[+] M. B. Applegate, Dr. A. Reeves, M. Paquette, Dr. B. Marelli, Prof. D. L. Kaplan, Prof. F. G. Omenetto
Department of Biomedical Engineering
Tufts University
Medford, MA 02155, USA
E-mail: fiorenzo.omenetto@tufts.edu

[+]Present Address: Department of Mechanical Engineering, The University of Texas at Austin, 204 E. Dean Keeton Street, Stop C2200, Austin, TX 78712-1591, USA

DOI: 10.1002/adfm.201502819

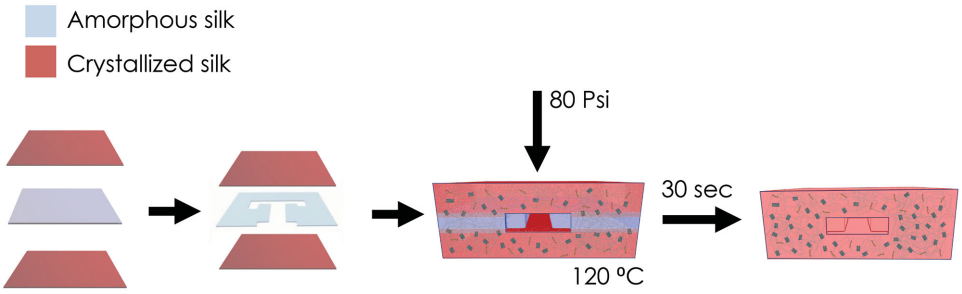

Figure 1. Schematic of the lamination method. The addition of an amorphous silk layer in between crystallized device layers will act as an adhesive. Patterning of the adhesive layer can then be used to spatially control adhesion in the adhered assembly. Samples will be treated using existing thermal processing protocols, with the application of 120 °C and 80 Psi of pressure for ≈30 s. This will cause interdiffusion and produce a weld at the layer interfaces, and lead to a fully crystallized final product.

including bilayers and microbubbles, with wide ranging applications.

Similar geometries have been investigated previously in silk and other materials.[22–24] However, these methods suffer from limitations in scale, poor stability, complex fabrication processes, and harsh chemistries.[25–27] Common approaches based on layer-by-layer deposition for fabricating capsule geometries are usually confined to dispersions, and require complex fabrication protocols to be applied in non-solution-based formats.[28–30] A recent method to develop silk microbubble geometries on a silicon wafer addresses some of these issues, but it is optimized for the nanoscale, is dependent on an inorganic wafer as a permanent substrate, and requires organic solvents which would lead to destruction of labile biological encapsulants.[22]

The application of silk thermal processing techniques to multilayer and bubble-like geometries addresses these concerns. We demonstrate a one-step method for rapid, high-throughput fabrication, using a silk-only approach that avoids substrate limitations and prevents solvent compatibility issues from arising. Additionally, we demonstrate the utility of this method for potential applications in drug delivery and transient electronics, and the stability of labile encapsulants throughout. This approach provides a versatile method for construction of complex multilayer structures in silk, which, with future work, may ultimately improve the utility of this material as a bridge between high technology and the biomedical sciences.

2. Lamination Method

The applicability of the reflow mechanism to spatially controlled lamination was first confirmed in order to validate the general experimental approach. Reflow in silk samples was investigated via Fourier-transform infrared spectroscopy and thermal gravimetric analysis, and the data were quantified using existing methods to confirm that reflow was occurring (**Figure 2**a). The beta-sheet crystallinity increased over time with the application of 120 °C and 80 Psi, while the water content decreased in a commensurate manner. This behavior is indicative of viscoelastic reflow as has been seen previously, and supports analysis in the context of the reflow mechanism.

The ability of silk adhesive to induce a strong interlayer bond was then analyzed by measuring the shear stress acting parallel to the bond cross section at the silk/silk interface with and without silk adhesive, in a geometry analogous to ASTM D3136 (i.e., mode II mechanical strength, Figure 2b). These tests were carried out on crystalline silk films (obtained by using previously established beta-sheet crystallization techniques) as well as amorphous control films, for which reflow bonding has been previously shown to be effective.[31–33] The crystallized films were stacked either with or without an internal amorphous silk adhesive layer, and then rapidly heated to 120 °C while 80 Psi of pressure was applied from the top. The adhered samples were evaluated by performing tensile testing (Figure 2c). The results revealed a lower bond strength when directly adhering two crystallized films, regardless of treatment, as compared to amorphous films. This matches previous results.[19] The bond was found to be stronger with the inclusion of an adhesive layer regardless of treatment. The results also correlate favorably with scanning electron microscope images (Figure 2d), where gaps are visible in the silk/silk interface region for crystallized film treatments, in contrast to a smooth interface for amorphous film lamination. The silk adhesive reduces these interfacial gaps in the crystallized samples by allowing reflow of the central film to weld the outer films together.

The ultimate bond strength obtained from different crystallization techniques is notably inconsistent due to a subset of the samples with silk adhesive exhibiting bulk material failures as opposed to interface failures at the adhesion sites. Crystallization methods which reduce residual water content in the individual films result in slightly weaker materials, and can explain the bulk failures, but also reflect the strength of the laminated interfaces, wherein the adhesive interface is occasionally stronger than the material itself.[32–34]

Regardless, the strength of the silk-adhesive-assisted bond is greater than 1100 kPa, which is suitable for survival in an in vivo setting, where minimal shear forces will affect the bond interface.[35] Additionally, the ability to spatially pattern silk adhesive layers introduces the possibility of topographically defined crystalline domains in multilayer silk devices and, consequently, affords additional control over device behavior in biological environments.

3. Method Characterization

The lamination method was next characterized to determine the resolution of spatial adhesion control (**Figure 3**a). In these

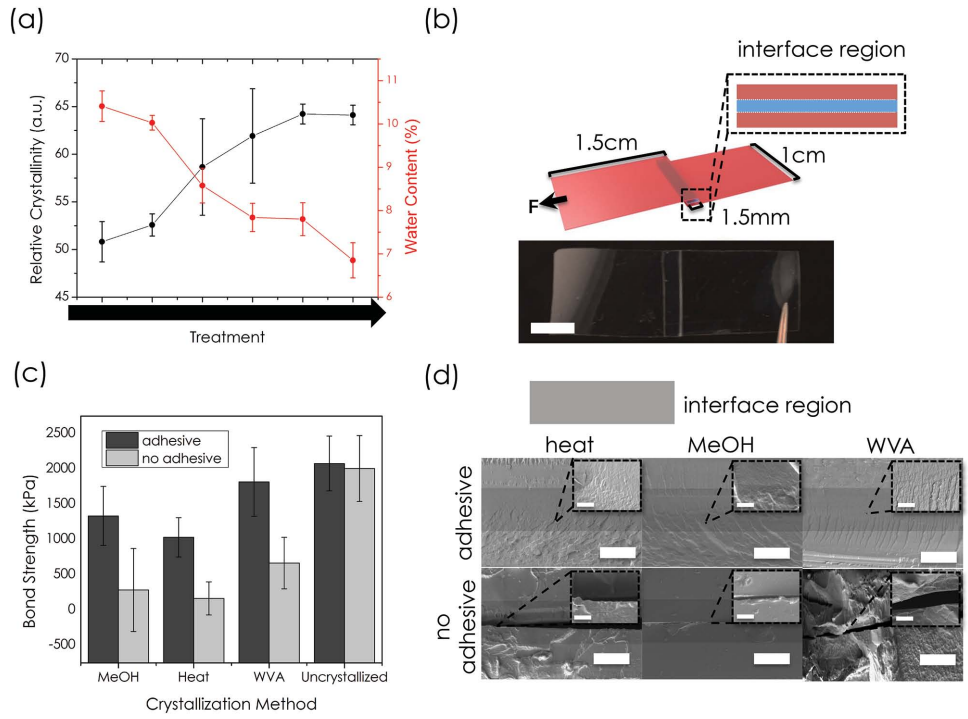

Figure 2. Process parameters and adhesion for the lamination method. a) Fourier-transform infrared spectroscopy and thermal gravimetric analysis of the crystallinity and water content of silk films as thermal processing is applied. b) Tensile testing schematic and sample, showing locations and sizes of layers used in test, as well as cross section of interface region. Crystallized silk is shown in red and amorphous silk is shown in blue. Geometry is similar to ASTM D3136. Scale bar on sample represents 0.5 mm. c) Quantified bond strength of tensile tested samples for $n = 6$, by crystallization condition. With the exception of the amorphous control group, all adhesive/no adhesive pairs are statistically significant by Tukey's test with $p < 0.05$. d) SEM cross-section images of tensile testing samples, showing the interface region near the center, with darker shading. Larger scale bars represent 60 μm, inset scale bars represent 2 μm, and highlight air gaps and fractures at the interface where present.

experiments, stacks of 40 μm thick films were laminated together, consisting of two pre-crystallized outer layers with an amorphous internal adhesive layer. The internal film contained arrays of ≈100 μm diameter holes fabricated by laser cutting, and blue food dye was added for contrast. Lamination produced sealed assemblies with microbubble architectures, as is shown in the images and cross section in Figure 3b. The effect of process parameters on the geometry of the laminated assemblies was analyzed using indexed image processing of the size and shape of individual microbubbles.

This experimental approach was first used to analyze the effect of pressure on the adhesion process. The pressure applied during lamination was varied from 40 to 400 Psi, and the decrease in individual bubble diameter as a consequence of reflow was monitored. This result is quantified in Figure 3c by calculating the remaining bubble diameter as a fraction of the initial diameter $((d_{initial} - d_{final})/d_{initial})$ to account for the variation in bubble size prior to treatment. The bubble diameter initially decreased sharply as the applied pressure was increased. Further increase in pressure, however, had little additional effect. This plateau in the results occurred at about 20% of the initial hole size, which corresponds to an approximate maximum travel distance of the viscoelastic-liquid silk of 40 μm from the edge of the microbubbles.

This behavioral trend can be explained in the context of the underlying silk reflow mechanism. The mechanism states that layer interdiffusion and travel distance of the viscoelastic liquid fibroin during reflow are governed by the time in that state, which is in turn a function of the heat propagation through the silk layers and crystallization kinetics.[19] Pressure is independent from heat propagation to first order. Therefore, pressure increase should consistently increase the travel distance of the reflowing protein, limited only by the crystallization kinetics. This limit was seen in the experiment as a plateau in travel distance once the adhesive layer had crystallized. From a process perspective, this result indicates that tight control of feature size via lamination will only be possible by taking the reflow distance into account. Sub-100 μm features should be achievable, however, with adequate process characterization. This result also has implications for existing thermal-reflow-based silk processing methods, as they should be able to be carried out independently of pressure as a control variable.[16,17,21,36]

Additional characterization was used to determine the effect of the thickness of the adhesive layer. A similar experiment to the pressure characterization was conducted, varying instead the thickness of the adhesive layer. The thickness was varied between 8 and 60 μm, while the external layers were kept fixed at a thickness of 40 μm. All samples were treated at 120 °C and 80 Psi for 20 s.

Fractional quantification of the bubble diameters from this experiment is presented in Figure 3d. The remaining bubble diameter ranged from 90% down to a minimum of 45%, indicating a decreased magnitude of effect for thickness

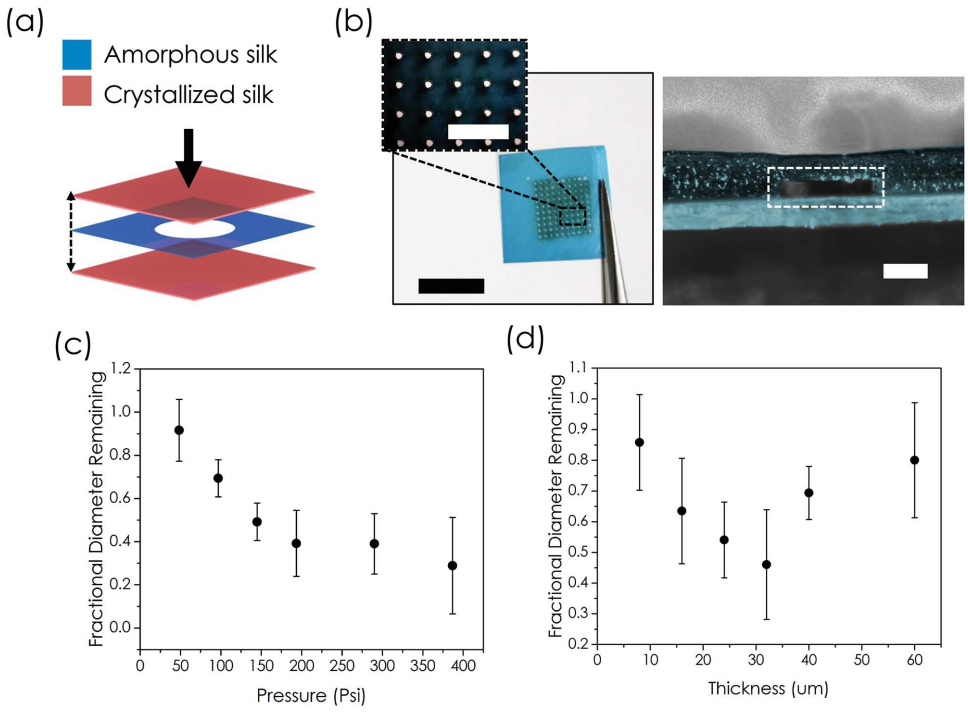

Figure 3. Characterization of spatial dimension of reflow and its effect on resolution. a) Schematic of sample design for characterization tests. Holes laser machined into the amorphous adhesive layer lead to microbubble architecture in the laminated films. b) Images of test samples. Array of 10×10 holes of 100 μm diameter was produced. After assembly, a clear bubble can be seen in the cross section. Scale bars represent 6 mm on the sample image, 1 mm on the inset, and 50 μm on the cross section. c) Remaining diameter as a fraction of the initial size for $n = 100$ bubbles adhered using different pressures. All means are statistically significant using Tukey's test $p < 0.05$. d) Remaining diameter as a fraction of the initial size for $n = 100$ bubbles adhered using different thicknesses of silk film adhesive. All means are statistically significant using Tukey's test $p < 0.05$.

as compared to applied pressure. A different trend was also observed in this case, where the remaining bubble diameter was largest for very thick and very thin adhesive layers, and smallest at intermediate sizes.

The reflow mechanism also provides a strong conceptual context for this result. The thickness of the adhesive layer has a direct effect on heat propagation through the silk layers during lamination, unlike the applied pressure. This means that the thickness of the adhesive is linked to the amount of time it will be in a viscoelastic liquid state. Very thick adhesive layers affect thermal diffusion and slow heat propagation, delaying the time at which the glass transition temperature is reached, limiting the time spent above it and the amount of reflow that occurs. In very thin adhesive layers, heat propagation is faster, leading to faster crystallization kinetics and once again less time for reflow. As a consequence, the highest reflow and correspondingly the smallest remaining diameters should occur at intermediate thicknesses, as was observed.

The characterization experiments and existing work suggest that lamination is effective across a wide range of temperatures, pressures, and silk thicknesses. The spatial application of silk adhesive should therefore be possible by a large number of existing positive and negative manufacturing techniques (such as laser machining, wet casting, inkjet printing, and dry etching of the silk material)[15,37] which would allow a variety of multilayer geometries to be fabricated across multiple scales.

4. Applications

This versatility makes the lamination method relevant for a number of biomedical applications. Recent advances in materials have generated completely bioresorbable devices which degrade in ambient conditions on predefined timescales, termed "transient" electronics.[38–40] This circumvents the need for device retrieval making transient devices advantageous for use as implants. Some of the materials used most often (i.e., magnesium conductors) in these devices degrade rapidly, however, and require passivation for stable operation on the desired timescales.[38,40,41] As a nonimmunogenic bioresobable material, silk is an ideal candidate for external passivation of these devices.

In order to protect and control the degradation of transient devices, either pocket geometries or direct passivation based on the lamination method can be used (**Figure 4**a). A magnesium antenna fabricated on a silk substrate was either encapsulated in a silk air pocket (1) or had a silk passivation layer directly applied to its surface via the lamination method (2). Measurement of the antenna response after protection showed a decrease in signal amplitude in the case of both methods, likely largely due to the effect of the additional silk material on the antenna coupling. The amplitude decrease was larger in the case of direct passivation, however, which may be due to the contact of the magnesium layer with liquid silk during reflow. Additionally, the air interface above the antenna in the pocket

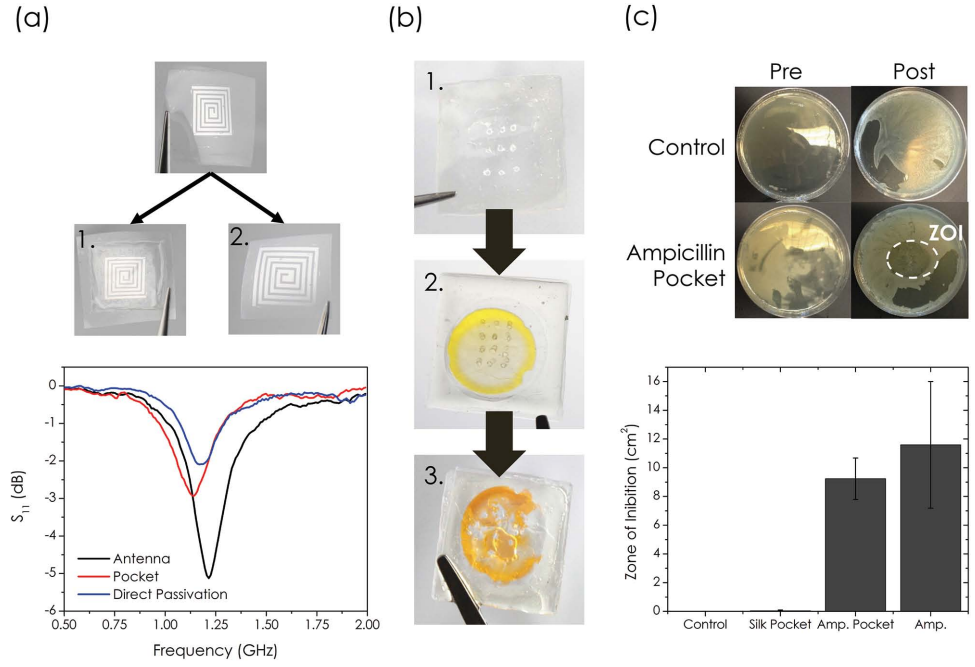

Figure 4. Applications of the lamination method in silk. a) Silk pockets for protection of transient electronics. Reflection response of a 1 cm RF antenna fabricated in magnesium on a silk substrate, before and after encapsulation in a silk pocket (1) or direct application of a silk passivation layer by the lamination method (2). b) Silk pockets for controlled release of proteins. (1) Image of crystallized silk film with machined holes, subsequently used to produce (2) a pocket containing an amorphous carrier film loaded with albumin fluorescein. (3) The same pocket after immersion in PBS for 20 min. c) Images and quantification of the zone of inhibition (ZOI) of growth on a bacterial lawn after treatment with antibiotic silk pockets for 30 min.

geometry may protect it further by decreasing device contact with water. Tuning the crystalline properties, silk thickness, silk structure, and number of layers could all affect the diffusion of water into the pocket and thus allow tunability of the device lifetime.

Additional applications exist in the field of drug delivery. Here, nanoparticles, micelles, and other geometries have enabled the controlled release of small molecules. These encapsulation geometries control release through both physical and chemical interactions between the drug and encapsulant, thereby acting as a diffusional barrier that can be tightly regulated due to high available surface area.[42–44] Delivery of protein pharmaceuticals in a similarly controlled manner remains a challenge, however, because the large size and highly labile nature of the payload makes loading into similar encapsulation geometries difficult.[45,46]

Protein pharmaceuticals can be entrapped in water-soluble silk films and fabricated into similar pocket or bubble geometries to address these issues. Figure 4b shows crystallized films that have had an array of small holes machined into them (1). These films are fabricated into a pocket containing an amorphous payload film loaded with fluorescein-albumin and immersed in water (2). Fabrication of the pocket is carried out by the introduction of the amorphous payload film, along with a separate amorphous adhesive layer, in between the outer crystallized films during pocket lamination (see the Experimental Section). This geometry releases the payload as the water diffuses into the pocket and dissolves the water-soluble silk carrier film (3). The number and location of the holes determine the release rate in this case. As with other encapsulation geometries, these pockets leverage the available surface area for diffusion (through number of holes), which should enable tight control of release rate. Chemical cross-linking of the protein payload to the silk carrier could further modulate the release rate and provide an additional mechanism for control.[47,48]

These applications would be severely limited, however, if the heat utilized to define the geometry damaged the biomolecules within the device. Silk possesses an inherent ability to stabilize labile compounds through a combination of molecular sequestration and limited hydration.[49] However, the effect of transient exposure to the high (120 °C) temperatures used in the lamination method has not been well studied. To test this behavior, silk pockets were fabricated by the lamination method with and without antibiotic doped silk and placed on bacterial lawns. Antibiotic release from the pockets led to bacterial death and inhibited bacterial ingrowth in a clear zone around the area where the pocket was placed (Figure 4c). Quantification of the size of this zone of inhibition through image analysis shows equivalent efficacy of both the antibiotic pockets and antibiotic solution, and no measured bacterial death in either control. This indicates that the explored welded geometries can be effectively doped to include bioactive compounds without loss of efficacy. Further extension of this idea to multilayer system could leverage multiple diffusion rates from different layers within the system. A multilayer silk device based on this principle could control the relative rate of release of multiple bioactive compounds, while simultaneously serving its defined purpose.

5. Conclusions

A method for spatial control of adhesion in multilayer silk fibroin laminates based on a thermal-reflow mechanism is described. This approach utilizes the application of heat (120 °C) and pressure (80 Psi) to crystallized silk device layers interdigitated with spatially patterned silk film adhesives, which establishes a strong (1100 kPa) bond between the layers. The adhesive layers can be patterned using previously demonstrated silk fabrication techniques allowing for the assembly of complex geometries including bilayers and microbubbles. With adequate process characterization and control of the adhesive thickness and process pressure, this method can be utilized to generate microscale features. The applications of geometries produced by this method are broad, spanning such diverse fields as transient electronics and drug delivery. Labile bioactive dopants in the layers of silk used to construct the device retain their efficacy, and can add an additional dimension of functionality to the completed devices. With future work, this method may ultimately allow for a number of additional silk-based technological devices, further improving the versatility of silk as a material at the interface of biology and high technology, while inspiring the adoption of these techniques to other biopolymers and naturally derived materials.

6. Experimental Section

Silk Processing: Films were cast from regenerated aqueous *B. mori* silk fibroin solution, the production of which has been previously described.[50] Briefly, *B. mori* cocoons were boiled in an (0.02 M) aqueous solution of sodium carbonate for 10 min to remove the immunogenic sericin protein, which acts as a glue holding the fibroin filaments together. The remaining fibroin was then rinsed thoroughly in deionized (DI) water and allowed to dry overnight. Next, the fibroin was dissolved in an (9.3 M) aqueous solution of lithium bromide at 60 °C for 3 h. The lithium bromide was subsequently removed from the solution via osmotic stress. The solution was placed into dialysis cassettes (Slide-a-Lyzer, Pierce, MWCO 3.5K) and dialyzed against water for 36 h. The resulting 5%–8% (w/v) aqueous solution was purified through centrifugation prior to casting. Finally, the silk films were cast onto poly(dimethylsiloxane) (PDMS) (Sylgard 184 Silicone Elastomer, Dow Corning Inc., Midland, MI) substrates at 1 mL in.$^{-2}$ and allowed to dry under ambient conditions, to produce films of ≈85 μm thickness.

Water Vapor Annealing: The films were placed in a vacuum oven (Fisher Scientific Isotemp Model 281A) with a (400 mL) container of DI water. The vacuum was set to −80 in. Hg, and the chamber was sealed for 24 h to treat the films by water vapor exposure.[31,32]

Heat Treatment: The films were placed in between a nickel shim and a (5 mm thick) PDMS (Sylgard 184 Silicone Elastomer, Dow Corning Inc., Midland, MI) layer and heated rapidly to 120 °C for 30 s, while 80 Psi of pressure was applied from the top using a custom built thermal press.[19,22]

Methanol Treatment: The films were placed in 100% methanol for 30 min to crystallize them.[33]

Lamination Procedure: The materials to be laminated were arranged as desired, before being rapidly heated to 120 °C and pressed together with 80 Psi of pressure for 30 s. For most applications, silk films were stacked between a PDMS (Sylgard 184 Silicone Elastomer, Dow Corning Inc., Midland, MI) layer for even pressure and an acid polished nickel shim substrate for even heating.

Mechanical Testing: Two (85 μm thick) films were overlapped in a modified lap-shear geometry (similar to ASTM D3136), with 1 cm × 1.5 cm silk films overlapped by 1.5 mm to produce an adhesion area of 150 mm^2. The films were pretreated using the previously described cross section of available silk film beta-sheet treatments and laminated with and without a (30 μm thick) silk adhesive layer in between at 120 °C and 135 Psi for 30 s. The films were then tested in tension (Instron 3360, Instron Inc., Norwood, MA) to failure, and the results were area normalized to determine the bond strength of the samples.

Microbubble Characterization Tests: Silk films were cast at 0.5 mL in.$^{-2}$ with and without the addition of blue food dye to produce films of 40 μm thickness. The transparent outer films were pretreated using the heat treatment method discussed above to crystallize them. The blue-dye loaded adhesive films were next laser machined to produce the test geometry. Briefly, an array of ≈100 μm diameter holes was created in each film via laser ablation. Amplified femtosecond pulses (Spitfire Pro, Spectra Physics, Santa Clara, CA) at a repetition rate of 1 kHz were focused onto the sample through a 10× microscope objective. A computer controlled micropositioning stage (Ludl Electronic Products, Hawthorne, NY) was used to control the spatial position of each hole and the exposure was set to 0.5 s per hole using an electronic shutter (Thorlabs, Newton, NJ). These films were then placed between two outer films and treated according to experimental conditions. In the first experiment, 120 °C was applied for 30 s, with effective pressures of ≈50, 100, 150, 200, 300, and 475 Psi. In the second experiment, 120 °C and 80 Psi were applied for 30 s, with adhesive film thickness varied to ≈8, 16, 24, 32, 40, and 60 μm by casting at 0.1, 0.2, 0.3, 0.4, 0.5, and 0.75 5 mL in.$^{-2}$. Complete optical image series were taken of each array before and after lamination. After postprocessing to reconstruct each array in its entirety, the images were analyzed via a custom developed MATLAB script to determine the diameter change in each feature. The features were compared in an indexed manner, so individual before and after comparisons were made.

Drug Release Pockets: Two silk films were cast at 0.75 mL in.$^{-2}$ and treated via the heat treatment method before being punctured (nine times) with a (22.5 gauge) needle to allow for diffusion. A (14 mm) diameter biopsy punch was used to remove the center from a third amorphous film to act as adhesive. A fourth payload film was cast at 0.75 mL sq.$^{-1}$ in.$^{-1}$, and loaded with 600 ng albumin-fluorescein (Sigma Aldrich, St. Louis, MO). The outer and adhesive films were then equilibrated to 80% RH and the drug film to 10%. The assembly was then laminated at 75 °C, and 40 Psi, for 30 s, before being immersed in 10× phosphate buffered saline (PBS) (Life Technologies, Carlsbad, CA) for 20 min to observe its behavior.

Antibiotic Pockets: 7% silk solution was mixed with ampicillin sodium salt (CAS 69-52-3, Sigma-Aldrich) at 1 mg mL^{-1}, and films were cast from the resulting mixture onto PDMS (Sylgard 184 Silicone Elastomer, Dow Corning Inc., Midland, MI) molds at 1 mL in.$^{-2}$ and allowed to dry at ambient conditions for 24 h. Silk films without antibiotic were cast at the same time as a control. The films were stored at 4 °C when not in use. The dried films were cut into 1 cm × 1 cm squares, and sealed on the edges at 120 °C for 5 s, with 150 Psi of pressure. *Escherichia coli* (Life Technologies, Carlsbad, CA) were grown in liquid culture with Tryptic Soy Broth (Becton, Dickinson and Company, Franklin Lakes, NJ) for 8 h, and then plated onto Tryptic Soy Agar (Becton, Dickinson and Company, Franklin Lakes, NJ). Bacterial lawns were then treated for 30 min in one of four groups: silk pocket, silk pocket + antibiotic, 1 mL antibiotic only, and no treatment. Lawns were allowed to develop overnight, and the zone of inhibition was measured after ≈18 h of growth using Image J software.

Acknowledgements

The authors would like to acknowledge support through an NSF-INSPIRE grant (DMR-1242240) and the Office of Naval Research (N00014-13-1-0596). M.A.B. acknowledges support through AFOSR, National Defense Science and Engineering Graduate (NDSEG) Fellowship, 32 CFR 168a.

Received: July 9, 2015
Revised: September 15, 2015
Published online: November 17, 2015

[1] S. Xu, Y. Zhang, L. Jia, K. E. Mathewson, K.-I. Jang, J. Kim, H. Fu, X. Huang, P. Chava, R. Wang, S. Bhole, L. Wang, Y. J. Na, Y. Guan, M. Flavin, Z. Han, Y. Huang, J. A. Rogers, *Science* **2014**, *344*, 70.
[2] Y. Sun, J. A. Rogers, *Adv. Mater.* **2007**, *19*, 1897.
[3] J. Viventi, D.-H. Kim, L. Vigeland, E. S. Frechette, J. A. Blanco, Y.-S. Kim, A. E. Avrin, V. R. Tiruvadi, S.-W. Hwang, A. C. Vanleer, D. F. Wulsin, K. Davis, C. E. Gelber, L. Palmer, J. Van der Spiegel, J. Wu, J. Xiao, Y. Huang, D. Contreras, J. A. Rogers, B. Litt, *Nat. Neurosci.* **2011**, *14*, 1599.
[4] H. Sirringhaus, *Science* **1998**, *280*, 1741.
[5] S. R. Forrest, *Nature* **2004**, *428*, 911.
[6] Y. Yang, F. Wudl, *Adv. Mater.* **2009**, *21*, 1401.
[7] F. G. Omenetto, D. Kaplan, *Nat. Photonics* **2008**, *2*, 641.
[8] D. Kim, J. Viventi, J. J. Amsden, J. Xiao, L. Vigeland, Y.-S. Kim, J. A. Blanco, B. Panilaitis, E. S. Frechette, D. Contreras, D. L. Kaplan, F. G. Omenetto, Y. Huang, K.-C. Hwang, M. R. Zakin, B. Litt, J. A. Rogers, *Nat. Mater.* **2010**, *9*, 511.
[9] S.-W. Hwang, D.-H. Kim, H. Tao, T. Kim, S. Kim, K. J. Yu, B. Panilaitis, J.-W. Jeong, J.-K. Song, F. G. Omenetto, J. A. Rogers, *Adv. Funct. Mater.* **2013**, *23*, 4087.
[10] J. J. Amsden, H. Perry, S. V Boriskina, A. Gopinath, D. L. Kaplan, L. D. Negro, F. G. Omenetto, *Opt. Express* **2009**, *17*, 21271.
[11] J. J. Amsden, A. Gopinath, L. D. Negro, D. L. Kaplan, F. G. Omenetto, *Chem. Eng.* **2009**, *7*, 9.
[12] E. M. Pritchard, X. Hu, V. Finley, C. K. Kuo, D. L. Kaplan, *Macromol. Biosci.* **2013**, *13*, 311.
[13] E. M. Pritchard, C. Szybala, D. Boison, D. L. Kaplan, *J. Controlled Release* **2010**, *144*, 159.
[14] E. Wenk, H. P. Merkle, L. Meinel, *J. Controlled Release* **2011**, *150*, 128.
[15] K. Tsioris, H. Tao, M. Liu, J. A. Hopwood, D. L. Kaplan, R. D. Averitt, F. G. Omenetto, *Adv. Mater.* **2011**, *23*, 2015.
[16] H. Tao, M. A Brenckle, M. Yang, J. Zhang, M. Liu, S. M. Siebert, R. D. Averitt, M. S. Mannoor, M. C. McAlpine, J. A. Rogers, D. L. Kaplan, F. G. Omenetto, *Adv. Mater.* **2012**, *24*, 1067.
[17] J. J. Amsden, P. Domachuk, A. Gopinath, R. D. White, L. D. Negro, D. L. Kaplan, F. G. Omenetto, *Adv. Mater.* **2010**, *22*, 1746.
[18] R. D. White, C. Gray, E. Mandelup, J. J. Amsden, D. L. Kaplan, F. G. Omenetto, *J. Micromech. Microeng.* **2011**, *21*, 115014.
[19] M. A. Brenckle, B. Partlow, H. Tao, D. L. Kaplan, F. G. Omenetto, *Biomacromolecules* **2013**, *14*, 2189.
[20] N. Agarwal, D. A. Hoagland, R. J. Farris, *J. Appl. Polym. Sci.* **1998**, *63*, 401.
[21] M. A. Brenckle, H. Tao, S. Kim, M. Paquette, D. L. Kaplan, F. G. Omenetto, *Adv. Mater.* **2013**, *25*, 2409.
[22] C. Ye, D. D. Kulkarni, H. Dai, V. V. Tsukruk, *Adv. Funct. Mater.* **2014**, *24*, 4364.
[23] A. G. Skirtach, A. M. Yashchenok, H. Möhwald, *Chem. Commun.* **2011**, *47*, 12736.
[24] C. S. Peyratout, L. Dähne, *Angew. Chem., Int. Ed. Engl.* **2004**, *43*, 3762.
[25] T. Leong, Z. Gu, T. Koh, D. H. Gracias, *J. Am. Chem. Soc.* **2006**, *128*, 11336.
[26] G. Stoychev, S. Turcaud, J. W. C. Dunlop, L. Ionov, *Adv. Funct. Mater.* **2013**, *23*, 2295.
[27] K. C. Wood, N. S. Zacharia, D. J. Schmidt, S. N. Wrightman, B. J. Andaya, P. T. Hammond, *Proc. Natl. Acad. Sci. USA* **2008**, *105*, 2280.
[28] C. M. Andres, I. Larraza, T. Corrales, N. A. Kotov, *Adv. Mater.* **2012**, *24*, 4597.
[29] J. T. Santini Jr., M. J. Cima, R. Langer, *Nature* **1999**, *397*, 335.
[30] A. R. Grayson, *Adv. Drug Delivery Rev.* **2004**, *56*, 173.
[31] B.-M. Min, L. Jeong, K. Y. Lee, W. H. Park, *Macromol. Biosci.* **2006**, *6*, 285.
[32] X. Hu, K. Shmelev, L. Sun, E.-S. Gil, S.-H. Park, P. Cebe, D. L. Kaplan, *Biomacromolecules* **2011**, *12*, 1686.
[33] M. Tsukada, Y. Gotoh, M. Nagura, N. Minoura, N. Kasai, G. Freddi, *J. Polym. Sci., Part B: Polym. Phys.* **1994**, *32*, 961.
[34] M. Tsukada, G. Freddi, M. Nagura, H. Ishikawa, N. Kasai, *J. Appl. Polym. Sci.* **1992**, *46*, 1945.
[35] C. O. Horgan, J. G. Murphy, *Proc. R. Soc. A* **2011**, *467*, 760.
[36] J. P. Mondia, J. J. Amsden, D. Lin, L. D. Negro, D. L. Kaplan, F. G. Omenetto, *Adv. Mater.* **2010**, *22*, 4596.
[37] H. Perry, A. Gopinath, D. L. Kaplan, L. D. Negro, F. G. Omenetto, *Adv. Mater.* **2008**, *20*, 3070.
[38] S. Hwang, H. Tao, D.-H. Kim, H. Cheng, J.-K. Song, E. Rill, M. A. Brenckle, B. Panilaitis, S. M. Won, Y.-S. Kim, Y. M. Song, K. J. Yu, A. Ameen, R. Li, Y. Su, M. Yang, D. L. Kaplan, M. R. Zakin, M. J. Slepian, Y. Huang, F. G. Omenetto, J. A. Rogers, *Science* **2012**, *337*, 1640.
[39] L. Yin, H. Cheng, S. Mao, R. Haasch, Y. Liu, X. Xie, S.-W. Hwang, H. Jain, S.-K. Kang, Y. Su, R. Li, Y. Huang, J. A. Rogers, *Adv. Funct. Mater.* **2014**, *24*, 645.
[40] R. Li, H. Cheng, Y. Su, S.-W. Hwang, L. Yin, H. Tao, M. A. Brenckle, D.-H. Kim, F. G. Omenetto, J. A. Rogers, Y. Huang, *Adv. Funct. Mater.* **2013**, *23*, 3106.
[41] S.-W. Hwang, X. Huang, J.-H. Seo, J.-K. Song, S. Kim, S. Hage-Ali, H.-J. Chung, H. Tao, F. G. Omenetto, Z. Ma, J. A. Rogers, *Adv. Mater.* **2013**, *25*, 3526.
[42] W. Li, F. C. Szoka, *Pharm. Res.* **2007**, *24*, 438.
[43] D. E. Owens, N. A. Peppas, *Int. J. Pharm.* **2006**, *307*, 93.
[44] G. Unsoy, R. Khodadust, S. Yalcin, P. Mutlu, U. Gunduz, *Eur. J. Pharm. Sci.* **2014**, *62*, 243.
[45] S. Mitragotri, P. A. Burke, R. Langer, *Nat. Rev. Drug Discovery* **2014**, *13*, 655.
[46] S. P. Schwendeman, R. B. Shah, B. A. Bailey, A. S. Schwendeman, *J. Controlled Release* **2014**, *190C*, 240.
[47] X. Wang, D. L. Kaplan, *Macromol. Biosci.* **2011**, *11*, 100.
[48] K. Tsioris, G. E. Tilburey, A. R. Murphy, P. Domachuk, D. L. Kaplan, F. G. Omenetto, *Adv. Funct. Mater.* **2010**, *20*, 1083.
[49] E. M. Pritchard, P. B. Dennis, F. Omenetto, R. R. Naik, D. L. Kaplan, *Biopolymers* **2012**, *97*, 479.
[50] D. N. Rockwood, R. C. Preda, T. Yücel, X. Wang, M. L. Lovett, D. L. Kaplan, *Nat. Protoc.* **2011**, *6*, 1612.